# Effect of ion orbit loss on the structure in the H-mode tokamak edge pedestal profiles of rotation velocity, radial electric field, density, and temperature

Weston M. Stacey

## Additional information on Phys. Plasmas

# Effect of ion orbit loss on the structure in the H-mode tokamak edge pedestal profiles of rotation velocity, radial electric field, density, and temperature

Weston M. Stacey

*Fusion Research Center, Georgia Institute of Technology, Atlanta, Georgia 30332, USA*

An investigation of the effect of ion orbit loss of thermal ions and the compensating return ion current directly on the radial ion flux flowing in the plasma, and thereby indirectly on the toroidal and poloidal rotation velocity profiles, the radial electric field, density, and temperature profiles, and the interpretation of diffusive and non-diffusive transport coefficients in the plasma edge, is described. Illustrative calculations for a high-confinement H-mode DIII-D [J. Luxon, Nucl. Fusion **42**, 614 (2002)] plasma are presented and compared with experimental results. Taking into account, ion orbit loss of thermal ions and the compensating return ion current is found to have a significant effect on the structure of the radial profiles of these quantities in the edge plasma, indicating the necessity of taking ion orbit loss effects into account in interpreting or predicting these quantities. © 2013 AIP Publishing LLC. [http://dx.doi.org/10.1063/1.4820954]

## I. INTRODUCTION

Since its discovery,[1] the (high-confinement) H-mode of operation in tokamak plasmas has been intensively investigated (e.g., Refs. 2–6). This interest arises not only because of its importance for the achievement of improved plasma confinement and other performance parameters but also because of the implications about the underlying physics inherent in the interesting structure that develops in the radial profiles of rotation, electric field, density, and temperature in the edge plasma when the H-mode is formed.[2] In the common tokamak configuration in which the plasma current and toroidal magnetic field are oppositely directed, the radial electric field and the carbon poloidal rotation velocity become negative (in a right-hand r-$\theta$-$\varphi$ system), and steep gradients in the density and temperature distributions are formed, all in a rather narrow "edge pedestal" region just inside the last closed flux surface (LCFS).

Numerous theoretical explanations have been proposed for the change in structure observed in the edge profiles during H-mode formation. It has been suggested that production of the negative well structure in the radial electric field is caused by non-ambipolar diffusive transport processes,[7] by the bifurcation in the momentum balance and in the poloidal rotation due to ion-orbit-loss in the edge plasma,[8] by the suppression of transport due to thermal instabilities by an increasing temperature gradient,[9] and by other means. The present reigning paradigm for the formation of the steep density and temperature gradients is that shear stabilization of microinstabilities due to the steep gradients (shear) in the radial electric field reduces the diffusive transport coefficients, requiring a steepening of density and temperature gradients in order to maintain the exhaust of heat and particles from the plasma core.[10,11] However, there is recent theoretical and experimental evidence that transport in the edge pedestal of H-mode plasmas has a strong non-diffusive component (e.g., Refs. 12–17) and that ion-orbit-loss has a significant effect on rotation in the plasma edge (e.g., Refs. 18–21).

Thus, while limiting values of temperature and density gradients are likely set by MHD (magnetohydrodynamic) instability limits on pressure gradients (e.g., Refs. 22 and 23), it would seem that before these MHD limits are reached, the density, temperature, rotation velocity, and electric field profiles in the edge plasma must be determined by the interaction of the edge plasma with external mechanisms (e.g., particle, energy and momentum losses,[18–21] and influxes[24,25]), the response to which must be determined by the plasma physics conservation constraints and the various transport processes taking place within the plasma. Understanding how the gradients are set prior to reaching the MHD limits is the key to understanding how to avoid these limits, or at least to control which MHD limits are reached.

The purpose of this paper is to present a model that relates the dependence of the density, temperature, rotation velocity, and radial electric field profiles in the edge plasma to the external sources and sinks of particles, energy, and momentum and to the momentum transport and energy conduction coefficients in the plasma edge. The particle sources and ion orbit losses determine the radial ion particle fluxes, which in turn affect the rotation velocities and thereby the radial electric field. The energy sources and sinks determine the radial energy fluxes of ions and electrons, and the heat conduction relations (surrogates for the fourth moment equations) determine the temperature gradients. The momentum balances govern the ion toroidal and poloidal rotation velocities and radial pressure gradient, and the ion density gradient is determined from the pressure gradient by subtracting the ion temperature gradient. The model used in this paper is based on "two-ion" fluid theory.

## II. A TWO-ION FLUID MODEL FOR THE STRUCTURE IN THE DENSITY, TEMPERATURE, ROTATION VELOCITY, AND ELECTRIC FIELD PROFILES IN THE PLASMA EDGE

### A. Radial ion flux

Integration of the steady-state particle continuity equation for species "j"

$$\nabla \cdot n_j \mathbf{V}_j \equiv \nabla \cdot \Gamma_j = S_{nbj} + n_{oj} n_e \langle \sigma_{ion} v \rangle_j \equiv S_{nbj}$$
$$+ n_e \nu_{ionj} \equiv S_j \qquad (1)$$

determines the flux-surface averaged radial component of the ion particle flux, which is denoted $\Gamma_{rj}$ and is usually outward except perhaps in the edge. The first term on the right is the neutral beam or pellet particle source rate of ions of species "j" and the second term is the ion particle source rate due to ionization of recycling or fueling neutral atoms of species "j." A similar equation obtains for all ion species present in the plasma, in particular, the main ion and impurity species with which we will be concerned in this paper.

Not all of this particle flux flows in the plasma subject to plasma transport processes because some of the ions are either born on drift orbits that pass outward through the LCFS or are carried radially outward in the flowing plasma until they access such orbits, at which point these ions are lost from the plasma across the separatrix or LCFS. A cumulative (with radius) fraction $F_{orbj}(r)$ of this total particle flux $\Gamma_{rj}$ resulting from external sources is lost from the edge region across the separatrix by ion-orbit-loss and by gradB drifting outward through the X-region (X-loss[26]) of either the fast beam ions or of the thermalized plasma ions, thereby reducing the actual flux of particles being transported radially outward in the plasma from that calculated by Eq. (1) to $\hat{\Gamma}_{rj} \equiv (1 - F_{orbj}) \Gamma_{rj}$.

In order to maintain charge neutrality, the loss of fast beam and thermalized plasma ions by ion-orbit-loss and X-loss must be compensated by either an inward current or a displacement current, which drives a negative radial electric field in the plasma edge to reduce the ion orbit loss. In this paper, we take into account the displacement current effect by using the measured radial electric field to calculate the ion orbit loss, but explicitly represent the return current that compensates those ions which are lost. We plan to explicitly treat the displacement current effect in a future paper.

Since the electrons are generally more effectively tied to field lines than are the ions, this current must be primarily carried by the ions.[18] Thus, the total inward current must compensate the ion-orbit-loss from both the "thermalized" plasma ions (main ion and impurities) and the fast neutral beam ions, $j_r = j_r^{iol} + j_r^{nbi}$. Because the ion orbit loss of the main (deuterium) ion species "j" is much greater than for the impurity (carbon) ion species "k,"[21] we make the approximation $j_r^{iol}(r) = -e_j F_{orbj} \Gamma_{rj} - e_k F_{orbk} \Gamma_{rk} \simeq -e_j F_{orbj}(r) \Gamma_{rj}(r)$ in calculating the return current. In this paper, we will be concerned with the ion orbit loss of thermalized plasma ions, which we consider to be likely to affect the edge plasma structure, but note that the loss of fast neutral beam ions (and one day alpha particles) should also be taken into account.

Assuming that the inward compensating current is carried by the main ion species, the net outward particle flux of the main ion species in the plasma due to loss of "thermalized" plasma ions (taking into account ion-orbit-loss and X-loss of outward flowing ions and the compensating inward current

of main ions from the scrape-off layer) is then $\hat{\Gamma}_{rj} \simeq (1 - F_{orbj}) \Gamma_{rj} - F_{orbj} \Gamma_{rj} = (1 - 2 F_{orbj}) \Gamma_{rj}$, where again $\Gamma_{rj}$ would be the outward main ion flux due to the neutral beam and recycling neutral sources in the absence of any ion-orbit-loss or X-loss of ions or compensating inward current. A negative value of $\hat{\Gamma}_{rj}$, as will occur in the edge when $F_{orbj} > 0.5$, indicates a net inward flux of the main ions. Since it is assumed that the compensating return current is carried by ions of the main species "j" and that ion orbit loss of the impurity species "k" is negligible, then ion orbit loss can be taken into account by replacing $\Gamma_{rj}$ with $\hat{\Gamma}_{rj} \equiv (1 - 2 F_{orbj}) \Gamma_{rj}$ for the main ions, but using the value of $\hat{\Gamma}_{rk} \equiv (1 - F_{orbk}) \Gamma_{rk} \simeq \Gamma_{rk}$ calculated from the continuity equation for the impurity ion species. The net radial flux of electrons is $\Gamma_{re} = z_j \hat{\Gamma}_{rj} + z_k \hat{\Gamma}_{rk}$.

It may be helpful to think of the radial particle fluxes of two categories of ions: (1) those that are on confined orbits and that are transported radially outward by diffusive and non-diffusive interactions within the plasma; and (2) those on loss orbits that constitute essentially instantaneous charge losses from the plasma when they reach a radius where they can access a loss orbit. This loss constitutes a reduction in the outflow of category 1 ions flowing radially in the plasma. The category 2 ions must be replaced immediately by an inward compensating current of cold ions from the scrape-off layer (SOL) flowing in the plasma and interacting with it (i.e., by a negative inward flow of category 1 ions) in order to maintain charge neutrality. The total outward ion flow of category 1 ions plus category 2 ions is unchanged by the ion orbit loss. However, the outward flow of category 1 ions is reduced first by the transfer of ion orbit loss ions to category 2 and then by the negative inflow of the compensating current category 1 ions. It is only the category 1 ions flowing in the plasma and interacting with it that are included in the plasma momentum balance equations and that thereby influence the plasma rotation and radial electric field (the category 2 ions are instantaneously removed from the plasma and influence it only via the effect on the category 1 ions just described).

## B. Ion rotation velocities

The continuity Eq. (1) can be combined with the momentum balance equation to obtain a balance among the inertial, pressure, viscous, electric field, VxB, collisional friction, and external source terms[27]

$$n_j m_j (\mathbf{V}_j \cdot \nabla) \mathbf{V}_j + \nabla p_j + \nabla \cdot \Pi_j = n_j e_j (\mathbf{E} + \mathbf{V}_j \times \mathbf{B}) + \mathbf{R}_j^1$$
$$+ (\mathbf{S}_j^1 - m_j \mathbf{V}_j S_j). \qquad (2)$$

In a two-ion-species plasma ("j" and "k"), the toroidal component of the momentum balance equation for species "j" can be written

$$B_\theta e_j \hat{\Gamma}_{rj} = n_j m_j (\nu_{dj} + \nu_{jk}) V_{\phi j} - n_j m_j \nu_{jk} V_{\phi k} - (M_{\phi j} + n_j e_j E_\phi^A) \qquad (3)$$

and the equation for the other ion species "k" is obtained by interchanging the "j" and "k" subscripts. (This formalism is readily generalized to multiple species by summing over "k.")

The quantity $\nu_{dj} \equiv \nu_{viscj}^{\phi} + \nu_{inertj}^{\phi} + \nu_{ionj} + \nu_{elcxj} + \nu_{anomj}^{\phi}$ is a composite toroidal momentum exchange frequency due to toroidal viscosity, toroidal inertia (Reynold's stress), ionization, elastic scattering plus charge exchange (defined similarly to $\nu_{ionj}$ but with the elastic + charge-exchange cross-section), and "anomalous" viscosity (due to turbulence, non-symmetric toroidal magnetic field, etc.), respectively, and can be determined experimentally[28] by solving Eq. (3) using measured rotation velocities. The quantity $\nu_{dj} + \nu_{jk}$ represents the total momentum exchange frequency for ions of

species "j." Justification for writing the viscous and inertial momentum transfer in this form is discussed in Refs. 12 and 29. $M_{\phi j} = M_{\phi j}^{nbi} + M_{\phi j}^{iol} + M_{\phi j}^{anom}$ is the toroidal momentum input from neutral beams, from the directionally preferential ion-orbit-loss and X-loss of "thermal" plasma ion momentum,[21] and from other sources. $E_{\phi}^{A}$ is the induced toroidal electric field, and the other quantities have their usual meaning.

Equation (3) and the corresponding equation for species "k" can be solved for

$$V_{\phi j} = \frac{\left[\dfrac{e_j B_\theta \hat{\Gamma}_{rj} + M_{\phi j} + n_j e_j E_\phi^A}{n_j m_j (\nu_{jk} + \nu_{dj})}\right] + \dfrac{\nu_{jk}}{(\nu_{jk} + \nu_{dj})}\left[\dfrac{e_k B_\theta \hat{\Gamma}_{rk} + M_{\phi k} + n_k e_k E_\phi^A}{n_k m_k (\nu_{kj} + \nu_{dk})}\right]}{\left[1 - \dfrac{\nu_{jk}\nu_{kj}}{(\nu_{jk} + \nu_{dj})(\nu_{kj} + \nu_{dk})}\right]} \tag{4}$$

and a similar equation with the subscripts "j" and "k" interchanged for $V_{\phi k}$. Here, in the case of the main ion species "j," $\hat{\Gamma}_{rj} = (1 - 2F_{orbj})\Gamma_{rj}$, taking into account both the ion orbit loss and the compensating inward current, but for the impurity species "k," $\hat{\Gamma}_{rk}$ is replaced by $\hat{\Gamma}_{rk} \equiv (1 - F_{orbk})\Gamma_{rk}$. Thus, the toroidal rotation for each species is driven by the terms in the numerator—the beam, ion-orbit-loss, and induced electric field toroidal momentum input to both species and the torque due to the radial particle fluxes of both species. The first term in the numerator represents the direct momentum drive to species "j," and the second term represents the momentum drive to species "k" that is transferred to species "j" by scattering. The response to these drives is determined by the momentum transport frequencies—interspecies, viscous, inertial, atomic physics, and anomalous—in the denominator.

The poloidal rotation velocities for the two ion species are determined by the poloidal component of the momentum

balance equations for each species. Using the Shaing-Sigmar form of the parallel viscosity[30] $\eta_{0j} = n_j m_j V_{thj} qRf_j(\nu_{jj}^*)$, $f_j \equiv \varepsilon^{-3/2}\nu_{jj}^*/(1 + \varepsilon^{-3/2}\nu_{jj}^*)(1 + \nu_{jj}^*)$, $\nu_{jj}^* \equiv \nu_{jj}qR/V_{thj}$ and neglecting poloidal asymmetries over the flux surface in density and flow, the poloidal momentum balance equation for ion species "j" may be written[31]

$$(-\nu_{viscj} + \nu_{jk} + \nu_{atomj})V_{\theta j} - \nu_{jk}V_{\theta k}$$
$$= -B_\phi \left\{ \frac{e_j}{n_j m_j}\hat{\Gamma}_{rj} - \nu_{viscj}\left(\frac{K^j T_j L_{Tj}^{-1}}{e_j B^2}\right)\right\}, \tag{5}$$

where $\nu_{viscj} \equiv qf_j V_{thj}/R$, $L_{Tj}^{-1} \equiv -T_j^{-1}\partial T_j/\partial r$, and $K^j \equiv \mu_{01}^j/\mu_{00}^j$ (the $\mu$'s are the Hirshman-Sigmar coefficients[31–33]). A similar equation with the "j" and "k" sub/super-scripts interchanged obtains for the "k" ion species. The two Eqs. (5) can be solved to obtain the poloidal rotation velocities

$$V_{\theta j} = \frac{\dfrac{-B_\phi}{\nu_{\theta j}}\left\{\left[-\nu_{viscj}\dfrac{K^j T_j}{e_j B^2}L_{Tj}^{-1} + \dfrac{e_j}{n_j m_j}\hat{\Gamma}_{rj}\right] + \dfrac{\nu_{jk}}{\nu_{\theta k}}\left[-\nu_{visck}\dfrac{K^k T_k}{e_k B^2}L_{Tk}^{-1} + \dfrac{e_k}{n_k m_k}\hat{\Gamma}_{rk}\right]\right\}}{\left[1 - \dfrac{\nu_{jk}\nu_{kj}}{\nu_{\theta j}\nu_{\theta k}}\right]}, \tag{6}$$

where $\nu_{\theta j} \equiv \nu_{viscj} + \nu_{jk} + \nu_{atomj} + \nu_{anom\theta j}$. A similar equation with the "j" and "k" sub/super-scripts interchanged results for $V_{\theta k}$. Again, for the main ion species "j," $\hat{\Gamma}_{rj} = (1 - 2F_{orbj})\Gamma_{rj}$; but for the impurity species "k," $\hat{\Gamma}_{rk}$ is replaced by $\hat{\Gamma}_{rk} \equiv (1 - F_{orbk})\Gamma_{rk}$. Equation (6) indicates that the poloidal rotation for each species is driven by the torques due to the radial particle fluxes and the temperature gradients of both species. The drive to species "j" is the sum of the torques acting directly on species "j" and

the torques acting on species "k", which are transferred to species "j" by scattering. The direction of the torques, hence the direction of the poloidal rotation, depends upon the direction of the toroidal magnetic field, the direction (in or out) of the radial particle fluxes and the direction of the temperature gradients. The response to this drive is determined by the momentum transport frequencies—interspecies, poloidal (parallel) viscous, atomic physics, and anomalous in the denominator.

## C. Radial electric field

Multiplying the radial component of the momentum balance for each species by $e_\sigma/m_\sigma$ for the species and summing over main ions, impurities, and electrons yields a generalized Ohm's law that governs the radial electric field[27]

$$
\begin{aligned}
E_r &= \eta j_r - (\mathbf{u} \times \mathbf{B})_r + \frac{\nabla_r(p_j + p_k)}{e(n_j + z_k n_k)} \\
&= -\eta e_j \Gamma_{rj} F_{orbj} - \frac{(V_{j\theta} B_\phi - V_{j\phi} B_\theta)}{(1 + n_k m_k/n_j m_j)} \\
&\quad - \frac{(V_{k\theta} B_\phi - V_{k\phi} B_\theta)}{(1 + n_j m_j/n_k m_k)} - \frac{(p_j L_{pj}^{-1} + p_k L_{pk}^{-1})}{e(n_j + z_k n_k)},
\end{aligned}
\tag{7}
$$

where $\mathbf{u}$ is the plasma mass velocity, $\eta \simeq 1.03 \times 10^{-4} Z_{eff}$ $\ln\Lambda/T_e^{3/2}(eV)\,\Omega - m$ is the Spitzer perpendicular plasma resistivity, and $j_r = -e_j\Gamma_{rj}F_{orbj}$ is the inward main ion current compensating the ion orbit loss and X-loss of fast beam ions and thermal plasma ions, again with $\Gamma_{rj}$ being the outward flow of main plasma ions that would result in the absence of ion orbit loss and X-loss (i.e., the solution of the continuity equation).

## D. Ion pressure and density gradient scale lengths

The toroidal and radial components of the momentum balance equations for two ion species "j" and "k" can be solved to obtain a pinch-diffusion relation for the radial particle fluxes, the flux surface averaged component of which may be written[12]

$$
\hat{\Gamma}_{rj} = n_j D_{jj}(L_{nj}^{-1} + L_{Tj}^{-1}) - n_j D_{jk}(L_{nk}^{-1} + L_{Tk}^{-1}) + n_j V_{rj}^{pinch}, \tag{8}
$$

where the "self-diffusion" coefficient is $D_{jj} \equiv (m_j T_j(\nu_{dj} + \nu_{jk}))/(e_j B_\theta)^2$, the "other-species-diffusion" coefficient is $D_{jk} = (m_j T_k \nu_{jk})/e_j e_k B_\theta^2$, and the pinch velocity representing electromagnetic and other external forces is

$$
\begin{aligned}
V_{rj}^{pinch} &= -\frac{M_{\phi j}}{n_j e_j B_\theta} - \frac{E_\phi^A}{B_\theta} + \frac{m_j \nu_{dj}}{e_j B_\theta}\frac{E_r}{B_\theta} \\
&\quad + \frac{m_j B_\phi}{e_j B_\theta^2}[(\nu_{dj} + \nu_{jk})V_{\theta j} - \nu_{jk}V_{\theta k}].
\end{aligned}
\tag{9}
$$

Equations (3) and (8) and a similar equation with subscripts "j" and "k" interchanged for ion species "k" can be solved for the value of the pressure gradient scale length $L_{pj}^{-1} \equiv -(\partial p_j/\partial r)/p_j$ that is required by momentum balance

$$
L_{pj}^{-1} = \frac{(e_j B_\theta)^2 \left[ \left\{ \dfrac{\hat{\Gamma}_{rj}}{n_j} - V_{rj}^{pinch} \right\} + \dfrac{m_j/e_j}{m_k/e_k}\dfrac{\nu_{jk}}{(\nu_{dk} + \nu_{kj})} \left\{ \dfrac{\hat{\Gamma}_{rk}}{n_k} - V_{rk}^{pinch} \right\} \right]}{m_j T_j(\nu_{dj} + \nu_{jk})[1 - (\nu_{jk}\nu_{kj}/(\nu_{dj} + \nu_{jk})(\nu_{dk} + \nu_{kj}))]}. \tag{10}
$$

Again, for the main ion species "j", $\hat{\Gamma}_{rj} = (1 - 2F_{orbj})\Gamma_{rj}$; but for the impurity species "k," $\hat{\Gamma}_{rk}$ is replaced by $\hat{\Gamma}_{rk} \equiv (1 - F_{orbk})\Gamma_{rk}$. The ion pressure gradient in the edge is seen to be driven by the electromagnetic forces in the pinch velocity and the radial particle fluxes corrected for ion orbit loss.

In using these equations to interpret experiments, it is practical to use the radial momentum balance to replace the impurity poloidal velocity (which is usually measured in DIII-D but not always in other experiments) with the impurity toroidal velocity (which usually is measured) and other terms to obtain

$$
\begin{aligned}
n_j V_{rj}^{pinch} &= -\frac{M_{\phi j}}{e_j B_\theta} - \frac{n_j E_\phi^A}{B_\theta} + \frac{n_j m_j}{e_j B_\theta} \\
&\quad \times \left[ (\nu_{jk} + \nu_{dj})\left(\frac{E_r}{B_\theta} + \frac{B_\phi}{B_\theta}V_{\theta j}\right) - \nu_{jk}V_{\phi k} \right].
\end{aligned}
\tag{11}
$$

If we take advantage of the fact that usually $L_{Tk}^{-1} \simeq L_{Tj}^{-1}$ for different ion species and further assume $L_{nk}^{-1} \simeq L_{nj}^{-1}$, we obtain a simplified expression for the main ion pressure gradient scale length that can be used to obtain a simple expression for the density gradient scale length

$$
\begin{aligned}
L_{nj}^{-1} &\equiv L_{pj}^{-1} - L_{Tj}^{-1} \simeq \frac{\hat{\Gamma}_{rj} - n_j V_{rj}^{pinch}}{n_j D_j} - L_{Tj}^{-1}, \quad \text{where} \\
D_j &\equiv \frac{m_j T_j \nu_{jk}}{(e_j B_\theta)^2}\left[1 + \frac{\nu_{dj}}{\nu_{jk}} - \frac{e_j}{e_k}\right].
\end{aligned}
\tag{12}
$$

## E. Ion and electron temperature gradient scale lengths

The temperature gradient scale lengths for the ion species and the electrons are determined by the heat conduction relations[14]

$$
L_{Tj}^{-1} = \frac{\left(Q_{rj}(1 - E_{orbj}) - 1.5 T_j \Gamma_{rj}(1 - F_{orbj})\right)}{n_j T_j \chi_j}, \tag{13}
$$

where the ion-orbit-loss fractions only obtain for the ions, not the electrons. This expression recognizes the reduction in both the outward total heat flux and outward convective heat flux due to ion orbit loss, but assumes that because of the much smaller SOL temperature that the inward convective heat flux from the SOL associated with the compensating inward ion current is negligible. The total energy fluxes satisfy the ion energy balance equations

$$\frac{\partial Q_{rj}}{\partial r} \equiv \frac{\partial}{\partial r}\left(q_j + \frac{3}{2}\Gamma_j T_j\right)$$

$$= q_{nbj} - q_{je} - n_j n_o^c \langle \sigma v \rangle_{cx} \frac{3}{2}(T_j - T_o^c) \qquad (14)$$

and the electron energy balance equation

$$\frac{\partial Q_{re}}{\partial r} \equiv \frac{\partial}{\partial r}\left(q_e + \frac{3}{2}\Gamma_e T_e\right) = q_{nbe} + q_{je} - n_e n_k L_k(T_e). \qquad (15)$$

The $q_{nb}$ terms represent neutral beam (or other) heating, $q_{je}$ is the ion-to-electron collisional energy transfer, and the last terms in Eqs. (14) and (15) represent charge-exchange cooling of the ions and radiation cooling of the electrons, respectively. The quantities $q_{j,e} \equiv n_{j,e} T_{j,e} \chi_{j,e} L_{T_{j,e}}^{-1}$ are the conductive heat fluxes.

While the density and temperature gradient scale lengths of Eqs. (12) and (13), along with the particle and energy flux Eqs. (1), (14), and (15), can be integrated to obtain density and temperature profiles, these profiles depend also on the boundary conditions at the last closed flux surface and at the inner boundary for the edge region calculation. Thus, for investigation of edge physics by comparison with experimental results, it is probably less ambiguous to compare gradient scale lengths.

## III. ION ORBIT LOSS FROM THE THERMALIZED ION FLUX FLOWING THROUGH THE PLASMA EDGE

In general, both fast beam ions (and fusion alpha particles) and thermalized plasma ions can execute lost orbits that cross the separatrix and interact with a material surface or plasma and recycling neutral atoms in the scrape-off layer, thus be lost from the confined plasma ion population. In small "spherical" tokamaks such as MAST,[34] it has been shown[18,35] that most of neutral beam injected ions are ion-orbit-lost before they slow down and that the rotational torque is produced by the radial return current necessary to maintain charge neutrality. On the other hand, for a larger more conventional tokamak such as DIII-D,[36] the beam ions are confined while they slow down to become part of the thermalized plasma ion population, which are ion-orbit-loss from the plasma edge.[19–21] We summarize in this section a computational methodology[21,26,37] that has been developed to treat the latter situation of ion-orbit-loss of thermalized ions from the plasma edge, but which could be extended to treat the loss of fast beam ions as well. We note that there is also an X-loss ion-orbit-loss mechanism,[38,39] but we have found this to compete for the same ions that would be loss by the ion-orbit-loss mechanism described below and will not explicitly consider it in this paper.

### A. Ion orbit loss of particles, energy, and ion momentum

We are concerned with the calculation of the loss of thermalized plasma ions, their energy, and their directed momentum by excursions from the flux surface on orbits that cross the LCFS and do not return to the plasma. (It is possible, of course, to define other loss surfaces and to calculate return fractions, but this is beyond the scope of the present paper.) Such processes take place for the thermalized plasma ions primarily in the edge

plasma, which is constantly replenished by outward ion particle, energy, and momentum fluxes from the core plasma.

Following the general computation procedure introduced by Miyamoto,[37] we have found[26,39] that at each flux surface in the plasma edge, there is a minimum ion speed $V_{\min(\zeta_0)}$ (or energy) for which an ion with a given directional cosine $\zeta_0$ with respect to the magnetic field can be lost, and that all ions with this $\zeta_0$ and speeds above this minimum will be lost. We have also found[26,39] by numerical calculation for several edge plasma distributions that $V_{\min(\zeta_0)}$ decreases with increasing plasma radius (decreasing distance to the last closed flux surface). As a given volume of plasma flows outward across the plasma edge, it first loses the highest energy ions and then loses successively lower energy ions as it flows across successively outward flux surfaces with successively lower ion temperatures. This loss is different for the different ion directions $\zeta_0$. So, the "hole" in the plasma velocity distribution extends progressively down to lower $V_{\min(\zeta_0)}$ with increasing radius, and the depth of the "hole" is different for different $\zeta_0$; i.e., the loss region is cumulative with increasing radius and directionally dependent.

The ion loss situation for a constant influx of plasma (from the core) flowing across the edge region and accumulating a progressively larger and direction-dependent loss region is different from the situation usually calculated of a static plasma with no source and a fixed loss cone. In the latter static, source-free situation, in-scattering of plasma from outside the loss cone is necessary to maintain the plasma loss rate. However, in the flowing plasma situation considered is this paper, the plasma loss rate is maintained by the influx of plasma from the core into the edge region. We do not consider in-scattering in this paper, based on estimates[26] that it would only slightly increase the calculated loss rates in most DIII-D discharges.

The details of ion particle and energy loss in a plasma flowing across the edge region in a tokamak have been worked out in Refs. 26 and 40, where detailed calculation results may be found. These results were extended in Ref. 21 to calculate the net directional momentum loss, hence the net oppositely directed momentum in the remaining plasma ions that are not lost (i.e., the intrinsic rotation produced by the directed momentum loss).

We use the conservation of canonical toroidal angular momentum

$$R m V_{\parallel} f_\varphi + e\psi = const = R_0 m V_{\parallel 0} f_{\varphi 0} + e\psi_0 \qquad (16)$$

to write the orbit constraint for an ion introduced at a location "0" on flux surface $\psi_0$ with parallel velocity $V_{\parallel 0}$, where $f_\varphi = |B_\varphi/B|$, $R$ is the major radius, and $\psi$ is the flux surface value. The conservation of energy and of poloidal angular momentum

$$\frac{1}{2}m(V_{\parallel}^2 + V_{\perp}^2) + e\phi = const = \frac{1}{2}m(V_{\parallel 0}^2 + V_{\perp 0}^2) + e\phi_0$$

$$\equiv \frac{1}{2}mV_0^2 + e\phi_0,$$

$$\frac{mV_{\perp}^2}{2B} = const = \frac{mV_{\perp 0}^2}{2B_0}, \qquad (17)$$

further require

$$V_\parallel = \pm V_0 \left[ 1 - \left| \frac{B}{B_0} \right| (1 - \zeta_0^2) + \frac{2e}{mV_0^2}(\phi - \phi_0) \right]^{1/2} \quad (18)$$

where $\phi$ is the electrostatic potential. The quantity $\zeta_0 = V_{\parallel 0}/V_0$ is the cosine of the initial guiding center velocity relative to the toroidal magnetic field direction. Using Eq. (18) in Eq. (16) and squaring leads to a quadratic equation in the initial ion velocity $V_0 = \sqrt{V_{\parallel 0}^2 + V_{\perp 0}^2}$,

$$V_0^2 \left[ \left( \left| \frac{B}{B_0} \right| \frac{f_{\varphi 0}}{f_\varphi} \zeta_0 \right)^2 - 1 + (1 - \zeta_0^2) \left| \frac{B}{B_0} \right| \right]$$
$$+ V_0 \left[ \frac{2e(\psi_o - \psi)}{Rmf_\varphi} \left( \left| \frac{B}{B_0} \right| \frac{f_{\varphi 0}}{f_\varphi} \zeta_0 \right) \right]$$
$$+ \left[ \left( \frac{e(\psi_0 - \psi)}{Rmf_\varphi} \right)^2 - \frac{2e(\phi_0 - \phi)}{m} \right] = 0. \quad (19)$$

Note that Eq. (19) is quite general with respect to flux surface geometry representation of $R$, $B$, and the flux surfaces $\psi$. By specifying an initial "0" location for an ion with initial direction cosine $\zeta_0$, and specifying a final location on the flux surface $\psi$, Eq. (19) can be used to determine if an ion with initial speed $V_0$ and direction cosine $\zeta_0$ can reach that final location on the flux surface $\psi$.

Thus, Eq. (19) can be solved for the minimum ion energy necessary for an ion located on an internal flux surface to cross the last closed flux surface at a given location (or to strike the chamber wall at a given location, etc.). All of the ions with speeds greater than this $V_{0\min}(\zeta_0)$ are able to cross the last closed flux surface. We will assume in this work that a fraction $R_{loss}^{iol}$ of these ions crossing the last closed flux surface strike the chamber or divertor wall, interact with plasma or neutrals in the scrape-off layer, etc., such as not to return back across the last closed flux surface into the confined plasma. (This loss fraction can in principle be calculated, but this will be deferred until a later paper.) We note that in actuality $R_{loss}^{iol}$ will depend on ion energy, direction $\zeta_0$ and location for crossing the LCFS, as well as the geometry and composition of the plasma chamber external to the LCFS, so that the use of a single number is an approximation made to illustrate the magnitude of this effect.

For the usual DIII-D anti-parallel current/magnetic field configuration, the quantity $V_{0\min}(\zeta_0)$ is very large for particles with parallel velocity components opposite to the direction of the toroidal magnetic field ($\zeta_0 < 0$), which execute banana orbits inside the flux surface, but becomes smaller with increasing $\zeta_0 > 0$ (i.e., as the particle velocity becomes more nearly aligned with the toroidal magnetic field direction). Some detailed calculations for a DIII-D shot are given in Refs. 21, 26, and 40. The particle charge "e" and mass "m" enter Eq. (19) as the ratio e/m, so, e.g., deuterium and carbon have the same minimum ion speed (but not the same minimum ion energy) for ion orbit loss.

The GTEDGE code, used to make the calculations discussed in Sec. III B, calculates $V_{0\min}(\zeta_0)$ using the electrostatic potential calculated by integrating the (experimental or other)

radial electric field, an approximate representation of the magnetic flux surface geometry described by $[R(r, \theta) = \bar{R} h(r, \theta)$, $B_{\theta,\varphi}(r, \theta) = \bar{B}_{\theta,\varphi}/h(r, \theta)$, $h(r, \theta) = (1 + (r/\bar{R})\cos \theta)]$, and an approximate flux surface representation $\psi(\rho) = R A_\varphi = \frac{1}{2} \left( \frac{\mu_0 I}{2\pi a^2} \right) \bar{R} \bar{a}^2 \rho^2$, which follows from Ampere's law and the assumption of uniform current density.

Since $V_{0\min}(\zeta_0)$ decreases with radius, cumulative (with increasing radius) particle, momentum, and energy loss fractions can be defined

$$F_{orb} \equiv \frac{N_{loss}}{N_{tot}} = \frac{R_{loss}^{iol} \int_{-1}^1 \left[ \int_{V_{0\min}(\zeta_0)}^\infty V_0^2 f(V_0) dV_0 \right] d\zeta_0}{2 \int_0^\infty V_0^2 f(V_0) dV_0}$$
$$= \frac{R_{loss}^{iol} \int_{-1}^1 \Gamma\left( 3/2, \varepsilon_{\min(\zeta_0)} \right) d\zeta_0}{2\Gamma(3/2)}, \quad (20)$$

$$M_{orb} \equiv \frac{M_{loss}}{M_{tot}} = \frac{R_{loss}^{iol} \int_{-1}^1 \left[ \int_{V_{0\min}(\zeta_0)}^\infty (mV_0\zeta_0) V_0^2 f(V_0) dV_0 \right] d\zeta_0}{2 \int_0^\infty (mV_0) V_0^2 f(V_0) dV_0}$$
$$= \frac{R_{loss}^{iol} \int_{-1}^1 \zeta_0 \Gamma\left( 2, \varepsilon_{\min(\zeta_0)} \right) d\zeta_0}{2\Gamma(2)}, \quad (21)$$

and

$$E_{orb} \equiv \frac{E_{loss}}{E_{total}} = \frac{R_{loss}^{iol} \int_{-1}^1 \left[ \int_{V_{0\min}(\zeta_0)}^\infty \left( \frac{1}{2} mV_0^2 \right) V_0^2 f(V_0) dV_0 \right] d\zeta_0}{\int_{-1}^1 \left[ \int_0^\infty \left( \frac{1}{2} mV_0^2 \right) V_0^2 f(V_0) dV_0 \right] d\zeta_0}$$
$$= \frac{R_{loss}^{iol} \int_{-1}^1 \Gamma\left( \frac{5}{2}, \varepsilon_{\min(\zeta_0)} \right) d\zeta_0}{2\Gamma\left( \frac{5}{2} \right)}, \quad (22)$$

where $\varepsilon_{\min}(\zeta_0) = mV_{0\min}^2(\zeta_0)/2kT$ is the reduced energy corresponding to the minimum speed for which ion orbit loss is possible, and an initially Maxwellian ion distribution has been assumed. The quantities $\Gamma(n)$ and $\Gamma(n, x)$ in Eqs. (20)–(22) are the gamma function and incomplete gamma function. The ion-orbit-loss-corrected ion particle and energy transport fluxes are then $\hat{\Gamma}(r) = \Gamma(r) \left( 1 - F_{orb}(r) \right), \hat{Q}(r) = Q(r) \left( 1 - E_{orb}(r) \right)$. For a given ion temperature, the loss fractions decrease with increasing ion mass because the minimum reduced energy for loss $\varepsilon_{\min}(\zeta_0)$ increases with ion mass.

We note that the effect of scattering collisions, which could both remove ions from loss orbits and scatter other confined ions into loss orbits, have been neglected in the above discussion. This neglect is valid when the time between collisions is long compared to the loss orbit transit time or $\nu_{jk}^* < 1$.

## B. Momentum loss and intrinsic rotation due to ion orbit loss

The effect of ion orbit momentum loss is somewhat different than for particle and energy loss. In the "standard" DIII-D anti-parallel current/toroidal field configuration, the usual preferential loss of $\zeta_0 > 0$ (counter-current) ions causes a residual $\zeta_0 < 0$ (co-current) intrinsic rotation in the edge plasma due to the preferential retention of co-current direction ions. The net co-current rotation velocity at any flux surface is determined by the cumulative net counter-current directed ion orbit loss that has taken place over all inner radii out to that flux surface in question. Determining the minimum loss speed $V_{\min(\zeta_0)}$ as described above leads to an expression for the equivalent net parallel counter-current momentum loss rate (or co-current momentum gain rate) due to ion orbit loss $\Delta M_{\phi j}^{iol} = |B_\phi/B|nm\nu_{dj}\Delta V_\parallel$, which can be used to compute the intrinsic co-rotation caused by ion orbit loss

$$
\begin{aligned}
\Delta V_\parallel(\rho) &= R_{loss}^{iol}2\pi\int_{-1}^{1}d\zeta_0\left[\int_{V_{\min}(\zeta_0)}^{\infty}(V_0\zeta_0)V_0^2f(V_0)dV_0\right]_\rho\\
&= 4\pi M_{orb}(\rho)\left[\int_0^{\infty}(V_0)V_0^2f(V_0)dV_0\right]_\rho\\
&= 2\frac{\Gamma(2)}{\pi^{1/2}}M_{orb}(\rho)V_{th}(\rho) = \frac{2}{\pi^{1/2}}M_{orb}(\rho)\sqrt{\frac{2kT_{ion}(\rho)}{m}}
\end{aligned}
\tag{23}
$$

with $M_{orb}$ given by Eq. (21). When the current and toroidal fields are anti-parallel, this net counter-current momentum loss (reduction) rate produces an intrinsic co-current rotation given by Eq. (23). Although ion species with the same charge-to-mass ratio e/m (e.g., deuterium and carbon) will have the same $V_{\min(\zeta_0)}$, the intrinsic rotation will decrease with ion mass because both $M_{orb}$ (because the minimum energy corresponding to the minimum loss speed scales with ion mass) and the thermal velocity decrease with ion mass, for the same ion temperature.

## IV. APPLICATION TO A DIII-D H-MODE DISCHARGE

A DIII-D[36] H-mode lower single null divertor plasma discharge with directed neutral beam injection and rotation (#123302 at 2600 ms: $P_{nb} = 8.66$ MW, I = 1.5 MA, B = −2.0 T, R = 1.75 m, a = 0.6 m, $\kappa = 1.84$, $q_{95} = 3.86$, and $n_C/n_D = 0.03$) was chosen to illustrate the use of the formalism presented in the previous sections. The experimental data, fitting procedures, error analyses, and various previous analyses are discussed for discharge #123302 in Refs. 26 and 41–43 and, in general, in Refs. 6, 26, 44 and 45. The background plasma representation, the recycling neutral calculation, and the solution of the equations of the previous sections were carried out in the GTEDGE code.

A few words are in order regarding the "interpretive" perspective taken in this section. If the transport coefficients

[the particle diffusion coefficients (actually the momentum transport frequencies that determine them) and the thermal diffusion coefficients] were known, then it would be possible to take a "predictive" approach and just solve the equations of Sec. III B with and without accounting for ion orbit loss and the compensating return current, and compare the two different solutions with each other and with experimental results to assess the effects of ion orbit loss on the structure in the edge pedestal. However, the transport coefficients are not known, and to guess at them for the purpose of solving the equations of Sec. III B with and without ion orbit loss corrections can lead to results that are somewhat ambiguous (e.g., if the transport coefficients are chosen to yield agreement in some fashion with measured profiles in other experiments, these coefficients must implicitly already compensate for some ion orbit loss). To avoid this ambiguity, we take an "interpretive" approach by using the equations of Sec. III B, with and without ion orbit loss corrections, to interpret experimental measurements in terms of the underlying transport mechanisms, with and without taking into account ion orbit loss and the compensating return current. These interpreted transport coefficients are then used to predict the profiles of other quantities for comparison with each other and with experiment.

### A. Radial ion flux

The radial ion flux calculated from the continuity equation using experimental data as input ($\Gamma_{rj}$) is shown in Fig. 1. Also shown are the radial ion fluxes corrected for ion orbit loss and the compensating return current ($\Gamma_{rj}[1 - 2F_{orbj}]$) for two values of the fraction of the ions on orbits crossing the separatrix which do not return to the confined plasma, $R_{loss}^{iol} = 100\%, 50\%$. Without ion orbit loss, the radial ion flux is outward and increasing with radius in the edge because of the ionization of recycling neutral atoms. However, taking into account the loss of outward flowing ions by ion orbit loss and the compensating inward flux of ions necessary to maintain charge neutrality, the radial ion flux decreases in the very edge and even becomes inward for a sufficiently large value of $R_{loss}^{iol}$.
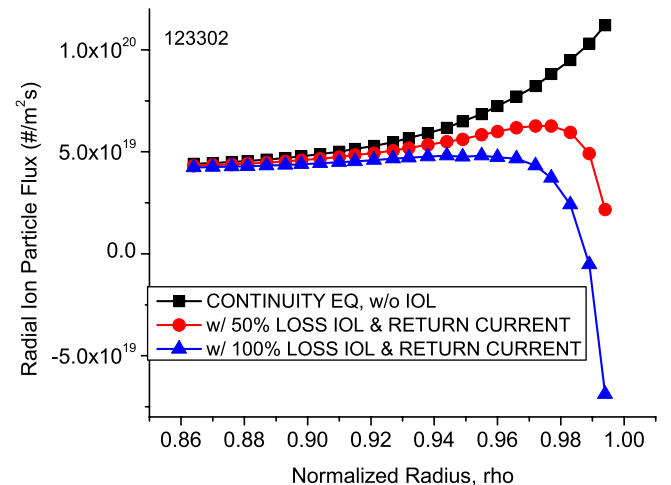


FIG. 1. Radial ion particle flux with ($R_{loss}^{iol} = 50\%$ and 100%) and without ($R_{loss}^{iol} = 0\%$) ion orbit loss and compensating return current.
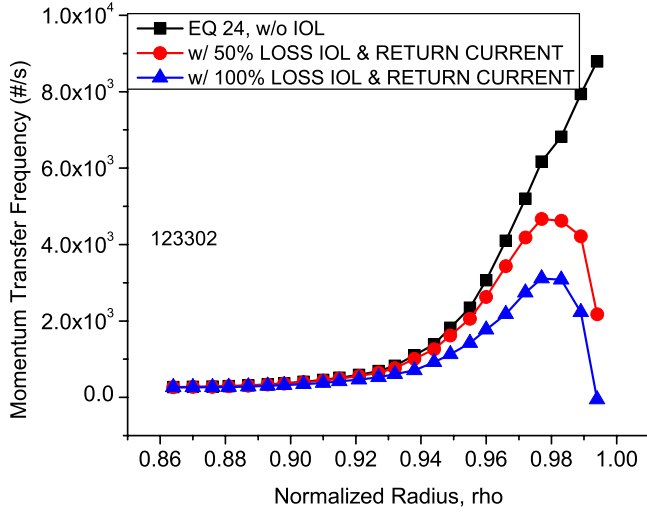
FIG. 2. Inferred experimental toroidal momentum transfer frequency with ($R_{loss}^{iol} = 50\%$ and $100\%$) and without ($R_{loss}^{iol} = 0\%$) ion orbit loss and compensating return current.

## B. Toroidal rotation

If the toroidal angular momentum transport frequencies, $\nu_{dj}$, were known and the toroidal velocities were measured for both the carbon impurity and deuterium main ions, then Eq. (4) for the two species could be evaluated and compared with the measured toroidal rotation velocities for the two ion species with and without accounting for ion orbit loss in order to evaluate the effect of ion orbit loss on toroidal rotation. However, the determination of a validated theoretical prediction of the $\nu_{dj}$ is an ongoing effort, and usually only the carbon impurity ion rotation velocity, $V_{\phi k}$, is measured (although there is recent progress[46] in determination of the deuterium toroidal rotation velocity from charge-exchange recombination (CER) data).

In order to move forward with an evaluation of the effect of ion orbit loss on toroidal rotation, we resort to a "bootstrapping" perturbation approach to infer reasonable values of the $\nu_{dj}$ and the "experimental" velocity for deuterium by first assuming a common toroidal momentum transport frequency $\nu_{d0} = \nu_{dj} = \nu_{dk}$ and summing the toroidal momentum balance Eq. (3) for the two ions species to obtain

$$\nu_{d0} = \frac{[\{\}_j + \{\}_k]}{[n_j m_j (V_{\phi k} + \Delta V_\phi) + n_k m_k V_{\phi k}]}, \quad (24)$$

where $\{\}_j \equiv \{B_\theta e_j \hat{\Gamma}_{rj} + M_{\phi j} + n_j e_j E_\phi^A\}$. We evaluate $E_\phi^A$ from measurement of the loop voltage, calculate the small beam momentum input from a simple analytical model, calculate the radial particle flux for deuterium from the continuity equation corrected by the ion orbit loss and compensating inward ion current, and assume the carbon radial particle flux is zero in equilibrium. The inferred momentum transfer frequency of Eq. (24) is plotted in Fig. 2 with and without taking into account ion orbit loss and the compensating return current. As can be seen, taking into account ion orbit loss and the compensating inward ion current substantially reduces the inferred experimental momentum transport rate in the edge, and the inferred toroidal momentum transport frequency even becomes inward ($<0$) just inside the separatrix for a sufficiently large value of $R_{loss}^{iol}$. It is clearly important to take ion orbit loss into account when interpreting the experimental data for the purpose of determining the experimental value of the momentum transport rate.

An equation for the quantity $\Delta V_\phi \equiv V_{\phi j} - V_{\phi k}$ can be determined by subtracting the two toroidal momentum balance Eqs. (3)

$$\Delta V_\phi = \frac{\left[ \left(1 - \frac{\nu_{kj}}{(\nu_{kj} + \nu_{dk})}\right) \frac{\{\}_j}{n_j m_j (\nu_{jk} + \nu_{dj})} - \left(1 - \frac{\nu_{jk}}{(\nu_{jk} + \nu_j)}\right) \frac{\{\}_k}{n_j m_j (\nu_{kj} + \nu_{dk})} \right]}{\left[1 - \frac{\nu_{jk} \nu_{kj}}{(\nu_{jk} + \nu_{dj})(\nu_{kj} + \nu_{dk})}\right]}. \quad (25)$$

A surrogate for the experimental deuterium velocity $V_{\phi j}^{"exp"} = V_{\phi k}^{meas} + \Delta V_{\phi 0}$ can then be constructed from the measured value of the carbon velocity $V_{\phi k}$ and Eq. (25) by using $\nu_{dj} = \nu_{dk} = \nu_{d0}$ given by Eq. (24) and Fig. 2. We improve the solution of the nonlinear set of Eqs. (24) and (25) iteratively, and find that the process converges when $|\Delta V_{\phi 0}/V_{\phi k}^{"exp"}| \ll 1$. Both $V_{\phi j}^{"exp"}$ and $V_{\phi k}^{meas}$ are plotted in Fig. 3 (the solid symbols); the small difference lends confidence to the use of the above perturbation technique for this discharge.

Next, we use $\nu_{dj}^* = \nu_{dk}^* = \nu_{d0}$ given by Eq. (24) to calculate the carbon and deuterium toroidal velocities from Eq. (4). While we can calculate the radial ion flux for deuterium, taking into account recycling neutral ionization sources and ion orbit loss, we are not presently able to make a similar calculation for the radial carbon flux, which is thus set to zero in the calculation. The calculated toroidal rotation velocities for deuterium and carbon are also plotted in Fig. 3 (the empty symbols). The calculated and "experimental" values agree rather well, providing some confidence in the self-consistency of the calculation.

When this calculation is repeated for $R_{loss}^{iol} = 50\%$ and $0\%$, the results are very similar to those shown in Fig. 3. Although the effects of ion orbit loss and return current on the radial particle flux and on the inferred momentum transfer frequency are significantly different for the different
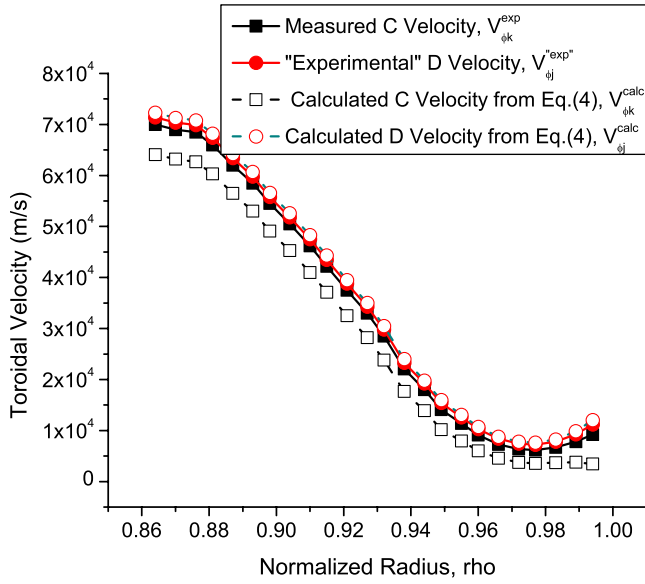
FIG. 3. Toroidal rotation velocity with $R_{loss}^{iol} = 100\%$ ion orbit loss and return current correction for discharge 123302.
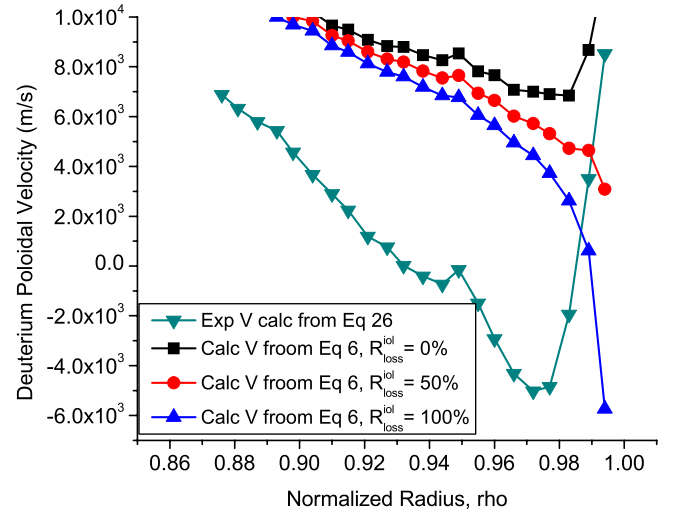


FIG. 4. Calculated and experimental deuterium poloidal rotation velocities with ($R_{loss}^{iol} = 50\%$ and 100%) and without ($R_{loss}^{iol} = 0\%$) ion orbit loss and compensating return current.

values of $R_{loss}^{iol}$, these two effects wash out in the calculation of the toroidal rotation velocity. This can be understood in terms of (i) the inference procedure described above compensating for any difference in the assumed and actual ion orbit loss with an inferred momentum transport frequency that reproduces the measured carbon toroidal rotation, (ii) the differences in the toroidal rotation velocities of carbon and deuterium being sufficiently similar that the perturbation theory calculation of the difference is valid, confirming the self-consistency of the methodology.

### C. Poloidal rotation

The poloidal velocity calculation is different in that previous experience indicates that the carbon and deuterium poloidal velocities may be quite different, so that a perturbation treatment such as used in Sec. IV B is not possible. Nor have we found a reliable way to infer the poloidal momentum transport frequency from experiment. Rather, a theoretical model for the poloidal angular moment transport frequency is used in calculations of the poloidal velocities of both species. The deuterium poloidal rotation velocity calculated from Eq. (6) is plotted in Fig. 4, with and without taking into account the ion orbit loss and compensating current effect on the radial particle flux of deuterium. Also plotted is an "experimental" value of the deuterium poloidal velocity constructed using the radial component of the momentum balance Eq. (2) for deuterium

$$V_{\theta j}^{"exp"} = \frac{1}{B_\phi}\left[B_\theta V_{\phi j}^{"exp"} - E_r^{exp} + \frac{1}{n_j^{exp} e_j}\frac{\partial p_j^{exp}}{\partial r}\right], \quad (26)$$

where the "experimental" value of the deuterium density is determined from the measured electron (Thomson scattering) and carbon (Charge Exchange Recombination) densities and the measured carbon temperature (assumed to be the same for deuterium), $V_{\phi j}^{"exp"}$ is calculated as described in Sec. IV B

using Eq. (25), and $E_r^{exp}$ is calculated from the radial component of the momentum balance Eq. (2) for carbon

$$E_r^{exp} = B_\theta V_{\phi k}^{exp} - B_\phi V_{\theta k}^{exp} + \frac{1}{n_k^{exp} e_k}\frac{\partial p_k}{\partial r}, \quad (27)$$

using the measured (CER) carbon rotation velocities, density, and temperature (the usual procedure for the determination of the experimental value of $E_r$). We emphasize that the "experimental" value shown in Fig. 4 is not a measured value but rather the difference in several measured values. Furthermore, the poloidal rotation calculation is based on a version of neoclassical theory. So, the main point to be made is that the different radial particle fluxes associated with different ion orbit losses produce different poloidal rotation velocities, not that theory agrees or disagrees with experiment.

Ion orbit loss and the compensating return current clearly can have a significant effect on the structure of the poloidal velocity in the edge plasma, but there is also clearly a difference between the theoretical and experimental structure independent of the treatment of ion orbit loss in H-mode shot 123302. This could be due to important phenomena (e.g., ion orbit loss of fast neutral beam ions,[34,35] up-down poloidal asymmetries in flux surface geometry, densities and flows,[29] etc.) not treated in the basic poloidal rotation theory used for the calculation or to the simplified representation of the flux surfaces ($\psi(\rho) = RA_\phi \approx (\mu_o I/4\pi a^2)R^2 a^2 \rho^2$) used in the ion orbit loss calculations.

### D. Transport coefficients

The differences in inferred toroidal momentum transfer frequencies shown in Fig. 2 translate directly into differences in the inferred experimental diffusion coefficients of Eq. (12), as shown in Fig. 5.

Taking ion orbit loss and return current into account significantly affects the pinch velocity of Eq. (9), both through the effect on the rotation velocities and the effect on the inferred momentum transfer frequency, as shown in Fig. 6.
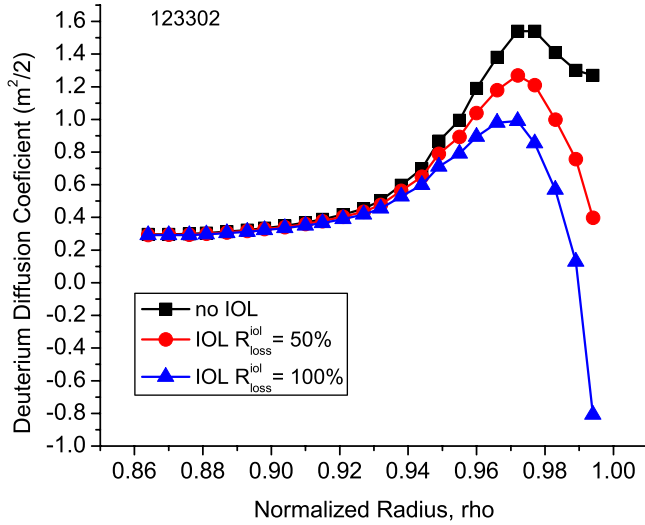
FIG. 5. Inferred experimental diffusion ion coefficient with ($R_{loss}^{iol} = 50\%$ and 100%) and without ($R_{loss}^{iol} = 0\%$) ion orbit loss and compensating return current.

An experimental $E_r$ determined from the carbon radial momentum balance Eq. (27) was used in the calculation. The smaller effect of ion orbit loss on the radial deuterium particle velocity ($V_{rad} \equiv \hat{V}_{rj} = \hat{\Gamma}_{rj}/n_j$) is also shown in Fig. 6. Clearly, the net radial velocity is the difference between much larger inward pinch velocities and outward diffusive velocities (or normalized forces).

## E. Pressure, temperature, and density gradients

In Fig. 7, the deuterium pressure gradients calculated from the momentum balance constraint of Eq. (12)

$$L_{pj}^{-1} \simeq \frac{\hat{\Gamma}_{rj} - n_j V_{rj}^{pinch}}{n_j D_j} \qquad (28)$$

with and without correction for ion orbit loss and return current are compared with the measured (Thomson and CER)
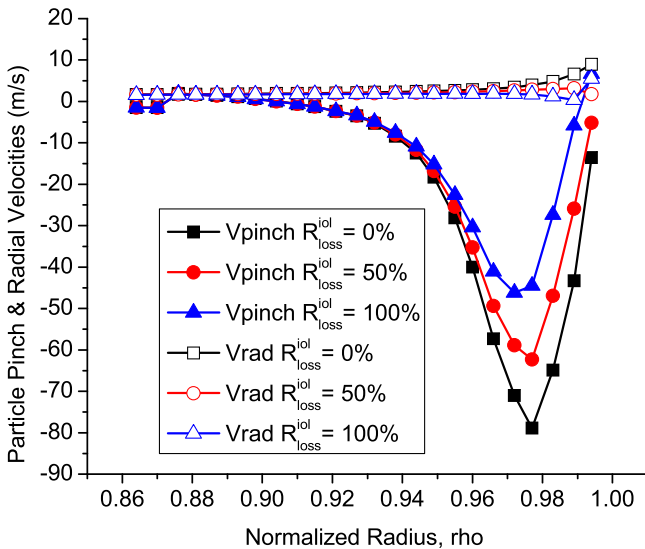
pressure gradient. The excellent agreement confirms the internal consistency of the calculation. Again, the fact that there is very little difference between the calculated pressure gradients with or without ion orbit loss (all four curves are literally on top of each other) is that the inference procedure used to obtain the toroidal momentum transfer frequency used in the evaluation of both $D_j$ and $V_{rj}^{pinch}$ compensates for any difference between the actual ion orbit loss and the value used in the calculation by an adjustment in the inferred toroidal momentum transport frequency.

If we knew the ion thermal diffusivity, the logarithmic ion temperature gradient could be calculated from Eq. (13) with and without taking into account the ion orbit correction. However, determination of a theory for the ion thermal diffusivity is still a matter of current research. Clearly, if we subtracted the measured log ion temperature gradient from the log ion pressure gradient determined from Eq. (2) and shown in Fig. 7, we would get a value of the log ion density gradient in very good agreement with the measured (Thomson + CER) log ion density gradient, because the experimental log ion pressure gradient was constructed by adding the measured log ion density and temperature gradients.

It is more instructive to rearrange Eq. (13) to obtain an expression for the experimental ion thermal diffusivity that would be inferred from the measured log ion temperature and density gradients,[26] with and without taking into account ion orbit loss corrections

$$\chi_j^{exp} = \frac{\left( Q_{rj}(1 - E_{orbj}) - 1.5 T_j \Gamma_{rj}(1 - F_{orbj}) \right)}{n_j T_j (L_{Tj}^{-1})^{exp}}. \qquad (29)$$

Here, the total ion particle and thermal fluxes, as determined from the continuity and thermal balance equations without ion orbit loss, are used, and the ion orbit loss corrections are shown explicity. (There is a cumulative with radius ion orbit loss fraction $E_{orbj}$ of the radial ion energy flux, as given by Eq. (21), as well as the ion orbit loss fraction $F_{orbj}$ of the
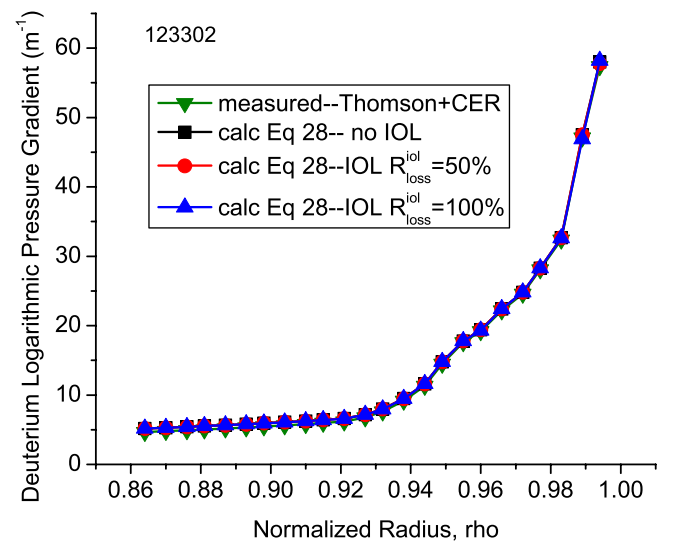


FIG. 6. Deuterium radial and pinch velocities with ($R_{loss}^{iol} = 50\%$ and 100%) and without ($R_{loss}^{iol} = 0\%$) ion orbit loss and compensating return current.



FIG. 7. Calculated and experimental deuterium logarithmic radial pressure gradient with ($R_{loss}^{iol} = 50\%$ and 100%) and without ($R_{loss}^{iol} = 0\%$) ion orbit loss and compensating return current.
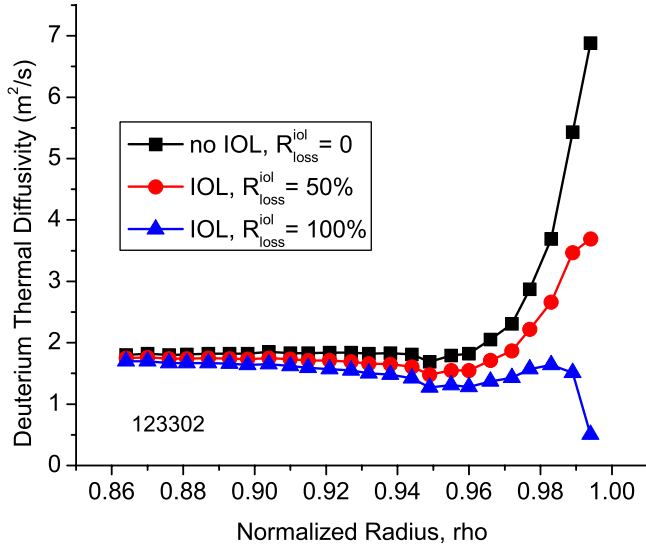
FIG. 8. Inferred deuterium thermal diffusivities with ($R_{loss}^{iol} = 50\%$ and 100%) and without ($R_{loss}^{iol} = 0\%$) ion orbit loss.

radial ion particle flux.) The inferred experimental ion thermal diffusivities, with and without ion orbit loss correction, are shown in Fig. 8. Clearly, taking ion orbit loss corrections to the ion energy and particle fluxes into account substantially changes the structure of the inferred experimental plasma ion thermal diffusivity in the plasma edge.

Since we have argued that there is no corresponding direct "electron orbit loss" because the smaller mass electrons do not execute drift orbits that cross the separatrix, the corresponding expression for the electrons would replace "j" with "e," have $E_{orbe} = 0$ and have a radial electron flux constrained by ambipolarity $\Gamma_{re} = \Gamma_{rj}(1 - F_{orbj}) + Z_k\Gamma_{rk}(1 - F_{orbk})$.

### F. Radial electric field

The radial electric field calculate from Eq. (7) for discharge 123302 with and without correction for ion orbit loss and return current is shown in Fig. 9. The contribution of the
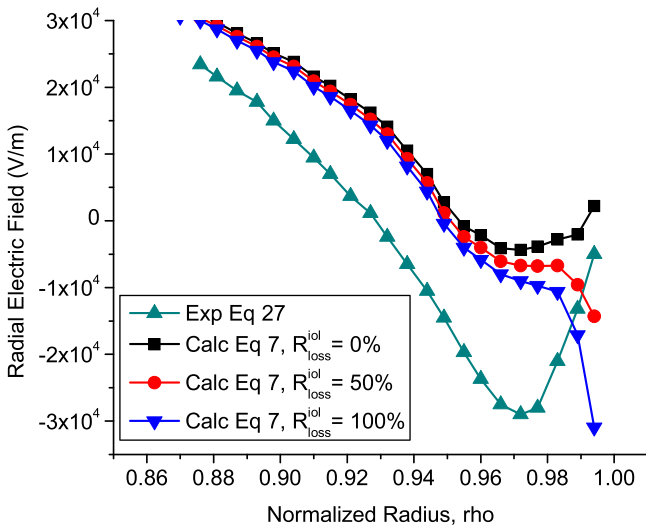


FIG. 9. Radial electric field calculated from Eq. (7) with ($R_{loss}^{iol} = 50\%$ and 100%) and without ($R_{loss}^{iol} = 0\%$) ion orbit loss for discharge 123302.

first (current) term is negligible, and the total electric field is the difference between the positive rotation contribution and the negative pressure gradient contribution. The rotation contribution is dominated by the deuterium poloidal rotation term which, as shown in Fig. 4, is not well calculated for this shot (possibly because of the neglect of neutral beam fast ion orbit loss), with the result that the agreement between the calculated and experimental (from the carbon radial momentum balance Eq. (27)) radial electric fields in the plasma edge is not too good. We note again that the "experimental" electric field is not a measured quantity but rather the difference of three measured quantities, so that the main point to be made by Fig. 9 is that the ion orbit loss has a significant effect on the radial electric field.

## V. DISCUSSION

A systematic methodology based on particle, momentum, and energy balance has been developed for investigating the effects of ion orbit loss of thermal ions on rotation, electric field, pressure, temperature, and density profiles in the edge pedestal. Ion orbit loss is found to affect the rotation profiles, which in turn affects the electric field and pressure profiles. Taking ion orbit loss into account is important in the interpretation of transport coefficients from measured density and temperature profiles in the edge pedestal.

The "two-ion" fluid particle, momentum, and energy conservation equations have been used to develop explicit expressions for the calculation of the radial pressure, temperature and density gradients, the profiles of toroidal and poloidal velocities, and the radial electric field profile in the plasma edge, taking into account the effects of ion orbit loss of thermalized plasma ions and the compensating return current. These expressions relate these quantities to the sources and losses of particles, momentum, and energy to/from the plasma, to the self-consistently calculated electromagnetic and thermodynamic forces acting within the plasma, and to the momentum and energy transport coefficients. The important transport parameters are shown to be the ion toroidal and poloidal momentum transport frequencies (viscous, inertial, atomic physics, anomalous) and the ion and electron thermal diffusivities, all of which are unknown, necessitating their inference from experimental data and the introduction of a theoretical poloidal momentum transport model.

In the plasma edge, the particle sources and ion orbit losses determine the radial ion particle fluxes, which in turn provide torques that, in part, determine the rotation velocities and thereby part of the radial electric field. These constitute the electromagnetic forces that determine the ion radial pressure gradient, which in turn partly determine the radial electric field. The energy sources and sinks determine the radial energy fluxes of ions and electrons, which in turn determine (via the heat conduction relations) the temperature gradients. The ion density gradient is the difference between these ion pressure and temperature gradients.

The formalism is applied to two DIII-D H-mode edge plasmas with an emphasis on illustrating the effect of ion

orbit loss of thermalized plasma ions and the compensating return current on the structure of these various profiles. Ion orbit loss of thermalized ions and the return current reduce the outward radial ion particle flux, and can even reverse it in the plasma edge. This ion orbit loss effect has a significant direct effect on the toroidal and poloidal rotation velocities and thereby an indirect effect on the radial electric field, density, and temperature profiles in the plasma edge. The thermal ions from neutral beam injection are included in the solution of the continuity equation for $\Gamma_{rj}$, but neither the ion orbit loss of fast beam ions nor the compensating return current of low energy ions is taken into account in this paper, which may account in part for some of the quantitative disagreement between the predicted and experimental rotation velocities and radial electric field.

In summary, ion orbit loss will affect interpretation of the value of the diffusive transport coefficients (thermal diffusivity, momentum transport frequency and resulting ion particle diffusion coefficient) from experiment (because it will affect the particle and energy fluxes that are flowing in the plasma), but it will not directly affect the basic diffusive transport mechanisms (neoclassical, ITG, etc.). However, ion orbit loss will affect the rotation and radial electric field in the edge (again by affecting the ion particle flux that is flowing in the plasma), which greatly affects the non-diffusive transport (e.g., pinch) in the edge. It is important to take these ion orbit loss effects into account in interpreting experimental values of diffusive transport coefficients from the measured profiles in order to avoid drawing the wrong conclusions about the agreement or disagreement of various theoretical predictions of the diffusive transport coefficients with experiment (e.g., that the diffusion coefficient is less than the neoclassical value). The ion pressure gradient is primarily determined by the pinch velocity and the particle diffusion coefficient (which in turn is determined by the momentum transport frequency), so it would be important to take ion orbit loss effects on the non-diffusive pinch into account in calculating the pressure gradient.

This investigation has focused almost exclusively on the effects of ion orbit loss of particles, acting through changes due to ion orbit loss in the radial particle fluxes flowing in the plasma. We note other important effects of ion orbit loss acting through changes in the radial energy[26] and momentum[21] fluxes flowing in the plasma due to ion orbit loss, as well as the effect of ion orbit loss on the distribution of particles, energy, and momentum into the scrape-off layer from the plasma core.[40]

Future work will incorporate a calculation of the ion orbit loss of fast neutral beam ions from deeper in the plasma and their compensating return current, a more realistic representation of the flux surface geometry, and a model for determining the loss fractions $R_{loss}^{iol}$.

## ACKNOWLEDGMENTS

[1]F. Wagner, G. Becker, K. Behringer, D. Campbell, A. Eberhagen, W. Engelhardt, G. Fussmann, O. Gehre, J. Gernhardt, G. V. Gierke, G. Haas, M. Huang, F. Karger, M. Keilhacker, O. Kluber, M. Kornherr, K. Lackner, G. Lisitano, G. G. Lister, H. M. Mayer, M. Meisel, E. R. Mueller, H. Murmann, N. Niedermeyer, W. Poschenrieder, H. Rapp, H. Rohr, F. Schneider, G. Siller, E. Speth, A. Staebler, K. H. Steuer, G. Venus, O. Vollmer, and Z. Yu, Phys. Rev. Lett. **49**, 1408 (1982).

[2]R. J. Groebner, K. H. Burrell, and R. P. Seraydarian, Phys. Rev. Lett. **64**, 3015 (1990).

[3]A. E. Hubbard, Plasma Phys. Controlled Fusion **42**, A15 (2000).

[4]F. Wagner, Plasma Phys. Controlled Fusion **49**, B1 (2007).

[5]C. F. Maggi, Nucl. Fusion **50**, 066001 (2010).

[6]W. M. Stacey, M.-H. Sayer, J.-P. Floyd, and R. J. Groebner, Phys. Plasmas **20**, 012509 (2013).

[7]S. I. Itoh and K. Itoh, Phys. Rev. Lett. **60**, 2276 (1988).

[8]K. C. Shaing and E. C. Crume, Phys. Rev. Lett. **63**, 2369 (1989).

[9]W. M. Stacey, Phys. Plasmas **9**, 3082 (2002).

[10]K. H. Burrell, Phys. Plasmas **4**, 1499 (1997).

[11]P. W. Terry, Rev. Mod. Phys. **72**, 109 (2000).

[12]W. M. Stacey, Contrib. Plasma Phys. **48**(1–3), 94 (2008).

[13]J. D. Callen, R. J. Groebner, T. H. Osborne, J. M. Canik, L. W. Owen., A. Y. Pankin, T. Rafiq, T. D. Rognlien, and W. M. Stacey, Nucl. Fusion **50**, 064004 (2010).

[14]W. M. Stacey, R. J. Groebner, and T. E. Evans, Nucl. Fusion **52**, 114020 (2012).

[15]H. Weisen, Y. Camenen, A. Salmi, T. W. Versloot, P. C. deVries, M. Maslow, T. Tala, M. Beurskens, C. Giroud, and JET-EFDA Team, Nucl. Fusion **52**, 114024 (2012).

[16]C. Angioni, Y. Camenen, F. J. Casson, E. Fabel, R. M. McDermott, A. G. Peeters, and J. E. Rice, Nucl. Fusion **52**, 114003 (2012).

[17]K. Kamiya, M. Honda, N. Miyato, H. Urano, M. Yoshida, Y. Sakamote, G. Matsunaga, N. Oyama, Y. Koide, Y. Kamada, K. Ida, and I. Murakami, Nucl. Fusion **52**, 114010 (2012).

[18]K. G. McClements and A. Thyagaraja, Phys. Plasmas **13**, 042503 (2006).

[19]J. S. deGrassie, R. J. Groebner, K. H. Burrell, and W. M. Solomon, Nucl. Fusion **49**, 085020 (2009).

[20]J. S. deGrassie, S. H. Mueller, and J. A. Bodeo, Nucl. Fusion **52**, 013010 (2012).

[21]W. M. Stacey, J. A. Boedo, T. E. Evans, B. A. Grierson, and R. J. Groebner, Phys. Plasmas **19**, 112503 (2012).

[22]P. B. Snyder, R. J. Groebner, A. W. Leonard, T. H. Osborne, and H. R. Wilson, Phys. Plasmas **16**, 056118 (2009).

[23]A. J. Webster, Nucl. Fusion **52**, 114023 (2012).

[24]M. A. Mahdavi, R. Maingi, R. J. Groebner, A. W. Leonard, T. H. Osborne, and G. Porter, Phys. Plasmas **10**, 3984 (2003).

[25]R. J. Groebner, M. A. Mahdavi, A. W. Leonard, T. H. Osborne, N. S. Wolf, G. D. Porter, P. C. Stangeby, N. S. Brooks, R. J. Colchin, and L. W. Owen, Nucl. Fusion **44**, 204 (2004).

[26]W. M. Stacey, Phys. Plasmas **18**, 102504 (2011).

[27]W. M. Stacey, *Fusion Plasma Physics*, 2nd ed. (Wiley-VCH, Weinheim, 2012), p. 90.

[28]W. M. Stacey and R. J. Groebner, Phys. Plasmas **15**, 012503 (2008).

[29]C. Bae, W. M. Stacey, and W. M. Solomon, Nucl. Fusion **53**, 043011 (2013).

[30]W. M. Stacey, A. W. Bailey, D. J. Sigmar, and K. C. Shaing, Nucl. Fusion **25**, 463 (1985).

[31]W. M. Stacey, Phys. Plasmas **15**, 012501 (2008).

[32]S. P. Hirshman and D. J. Sigmar, Nucl. Fusion **21**, 1079 (1981).

[33]B. Kim, P. H. Diamond, and R. J. Groebner, Phys. Fluids B **3**, 2050 (1991).

[34]R. J. Akers, P. Helander, A. Field, C. Brickley, D. Muir, N. J. Conway, M. Wisse, A. Kirk, A. Patel, A. Thyagaraja, C. M. Roach, and MAST Team (International Atomic Energy Agency, Vienna, 2005), EX4-4.

[35]P. Helander, R. J. Akers, and L.-G. Ericksson, Phys. Plasmas **12**, 112503 (2005).

[36]J. Luxon, Nucl. Fusion **42**, 614 (2002).

[37]K. Miyamoto, Nucl. Fusion **36**, 927 (1996).

[38]C. S. Chang, S. Kue, and H. Weitzner, Phys. Plasmas **9**, 3884 (2002).

[39]W. M. Stacey, Phys. Plasmas **18**, 122504 (2011).

[40]W. M. Stacey, Nucl. Fusion **53**, 063011 (2013).

[41]T. E. Evans, K. H. Burrell, M. E. Fenstermacher *et al.*, Phys. Plasmas **13**, 056121 (2006).

[42]W. M. Stacey and T. E. Evans, Phys. Plasmas **13**, 112506 (2006).
[43]W. M. Stacey and T. E. Evans, Nucl. Fusion **51**, 013007 (2011).
[44]W. M. Stacey and R. J. Groebner, Phys. Plasmas **14**, 012501 (2007).

[45]W. M. Stacey and R. J. Groebner, Phys. Plasmas **17**, 112512 (2010).
[46]B. A. Grierson, K. H. Burrell, W. M. Solomon, and N. A. Pablant, Rev. Sci. Instrum. **81**, 10D735 (2010).